

UC Santa Barbara

UC Santa Barbara Previously Published Works

Title

A measure of near-surface fluid motions that predicts air-water gas transfer in a wide range of conditions

Permalink

<https://escholarship.org/uc/item/2c3975ss>

Journal

Geophysical Research Letters, 32(4)

ISSN

0094-8276

Authors

Turney, D E
Smith, W C
Banerjee, S

Publication Date

2005-02-01

Supplemental Material

<https://escholarship.org/uc/item/2c3975ss#supplemental>

Peer reviewed

2 A measure of near-surface fluid motions that predicts air-water gas 3 transfer in a wide range of conditions

4 Damon E. Turney

5 Bren School of Environmental Science and Management, University of California, Santa Barbara, California, USA

6 Walter C. Smith

7 Department of Mechanical and Environmental Engineering, University of California, Santa Barbara, California, USA

8 Sanjoy Banerjee

9 Department of Chemical Engineering, University of California, Santa Barbara, California, USA

10 Received 4 October 2004; accepted 7 January 2005; published XX Month 2005.

12 [1] Air-water gas transfer impacts many important
13 biogeochemical processes, yet current understandings
14 involve large uncertainty. This arises because the process
15 depends on a complex interaction between molecular
16 diffusion and fluid motions that has not been adequately
17 characterized. Here we show the first experimental support
18 for a mechanistic model that relates near-surface motions to
19 gas transfer coefficients over a range of flow conditions,
20 including those leading to breaking wavelets. We find that
21 the square root of the root mean square surface-velocity
22 divergence varies linearly with gas transfer coefficients, as
23 predicted by theory, and also with mean square surface
24 slope. Besides advancing the understanding of the
25 mechanisms governing air-water gas transfer, these results
26 suggest easy-to-measure parameters that could, with further
27 investigation, provide gas transfer coefficients in field
28 settings. **Citation:** Turney, D. E., W. C. Smith, and S. Banerjee
29 (2005), A measure of near-surface fluid motions that predicts air-
30 water gas transfer in a wide range of conditions, *Geophys. Res.*
31 *Lett.*, 32, LXXXXX, doi:10.1029/2004GL021671.

33 1. Introduction

34 [2] Early interest in the subject of air-water gas transfer
35 arose from the need to understand the aeration of anoxic
36 waters, and has continued due to the need to track dissolved
37 pollutants, greenhouse gases, and other geochemical com-
38 pounds. A large amount of literature exists on the subject,
39 including recent reviews [Banerjee and MacIntyre, 2004].
40 In spite of this body of work, the mechanisms that drive the
41 process remain poorly understood and consequently pre-
42 dictions have large uncertainty. For example, widely used
43 predictive models of the gas transfer process commonly
44 differ by factors of three or more, and contain poorly
45 understood non-linearities [Banerjee and MacIntyre,
46 2004]. This translates to uncertainties of at least 300% in
47 recent attempts to calculate a net oceanic CO₂ uptake
48 [Donelan et al., 2002; Takahashi et al., 2002]. Such
49 uncertainty is due to the highly variable nature of correlat-
50 ing factors, e.g., wind, waves, surfactants, and thermal
51 convection or stratification. The purpose of this letter is to
52 report experimental support for a mechanistic model of air-

water gas transfer that accurately predicts the rates in a wide
range of conditions. 53 54

[3] Previous attempts to develop mechanistic models of
the process [Danckwerts, 1951; Komori et al., 1993; Siddiqui
et al., 2004; Zappa et al., 2001] have relied on surface-
renewal models. However, these models are limited by
ambiguity in defining their central parameter — the time-
scale of renewal — and consequently much tuning of
parameters is needed for predictions to agree with measure-
ments. An alternative model, termed the “surface diver-
gence” model, has been developed [Chan and Scriven, 63
1970; McCreedy et al., 1986]. This model recently was
shown to agree with data from a grid-stirred tank without
wind [McKenna and McGillis, 2004] and with direct
numerical simulations at low wind speeds [Banerjee et al.,
2004]. This letter builds on these results by showing
experimental support for the model at low and intermediate
wind speeds, with breaking wavelets arising at the interme-
diate wind speeds. This is an important advance, since
similar conditions are ubiquitous in the environment and
yet it is not clear how they affect air-water gas transfer. 73

2. Conceptual Model 74

[4] The gas transfer coefficient, k , is defined as 75

$$k \equiv \frac{N}{(c_b - c_{eq})} \quad (1)$$

where N is the gas flux density across the interface, c_{eq} is
the equilibrium concentration at the interface, and c_b is the
bulk concentration. Because the molecular diffusivities, D ,
of most gases in water are $\sim O(10^{-9} \text{ m}^2/\text{s})$, the main
resistance to transfer lies in a very thin layer, $\sim O(10 \text{ }\mu\text{m})$,
on the water side of the interface [Jahne and Haussecker,
1998]. In this layer a combination of molecular diffusion
and convective liquid motions control the gas transfer rate. 84

[5] Reliable models have been proposed for very low
wind speeds where wavelets do not break [Banerjee et al.,
2004]. However, when short wavelets appear, gas transfer
coefficients become more sensitive to wind speed and the
situation is poorly understood. This transition is usually
reported to occur when the ten-meter-height wind speed,
 U_{10} , is greater than 3.5 m/s. In this wavelet regime,
molecular diffusion and near-surface motions should still 92

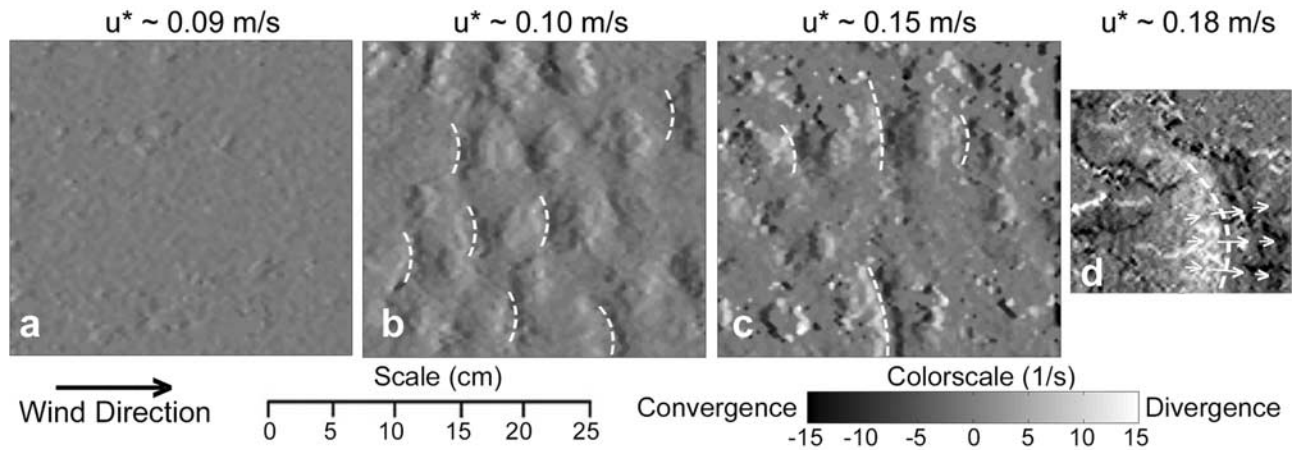


Figure 1. (a–d) Plan view images of instantaneous surface divergence under progressively higher wind stress. Example wave crests are drawn in with dashed white lines, as determined from the raw overhead photographs. The camera had a smaller field of view for $u^* \sim 0.18, 0.19, \text{ and } 0.21 \text{ m/s}$, as seen in (d). Example surface velocity vectors are shown in (d), but note that the actual density of DPIV velocity vectors for each image was 237×253 .

93 control the transfer rate but much uncertainty exists as to
 94 which motions are important and how to model predictions.
 95 The surface divergence model, mentioned earlier, suggests
 96 that a useful measure is the instantaneous surface divergence,

$$\gamma = (du'/dx + dv'/dy) \quad (2)$$

98 where u' and v' are the interface-tangential velocity
 99 fluctuations. The root mean square (rms) surface divergence
 100 is $(\overline{\gamma^2})^{1/2}$, where the overbar denotes an ensemble average.
 101 In the thin liquid layer near the surface where the main
 102 resistance to transfer exists, γ is equal to the interface-
 103 normal-velocity gradient [Banerjee and MacIntyre, 2004].
 104 A simplified form of the surface divergence model is

$$\bar{k} = C\sqrt{D(\overline{\gamma^2})^{1/2}} \quad (3)$$

106 where \bar{k} is the average gas transfer coefficient and C is a
 107 constant $\sim O(1)$ [Chan and Scriven, 1970; Csanady, 1990;
 108 McCready et al., 1986; Banerjee, 1990]. The term $(\overline{\gamma^2})^{1/4}$ is
 109 termed “the square root of the rms surface divergence”. As
 110 mentioned earlier, equation (3) was recently verified in
 111 direct numerical simulations and in a laboratory with grid-
 112 stirred turbulence. The strength of this model is its
 113 mechanistic origin and the scaling arguments that suggest
 114 $(\overline{\gamma^2})^{1/4}$ generically accounts for all motions, e.g., wave,
 115 turbulent, or viscous motions. In this report we experimen-
 116 tally test equation (3) under windy conditions for the first
 117 time, including intermediate wind speeds with short break-
 118 ing wavelets, sometimes called microbreaking waves.

119 3. Experimental Setup

120 [6] The experiments were conducted in a linear wind-
 121 wave channel of height 31 cm, width 71 cm, and length
 122 11.5 m. Water height was constant at 9.5 cm. The water
 123 surface was continuously cleaned with a surface vacuum
 124 during experiments and for 30 minutes prior to experiments.
 125 Bulk water velocity was steady at 1 cm/s, co-current with
 126 the wind.

[7] The gas transfer coefficient, \bar{k} , was measured by the
 127 streamwise gradient in dissolved oxygen concentration at
 128 steady state, similar to previous studies [McCready and
 129 Hanratty, 1985]. The equation $\bar{k} = \Gamma/\Delta x \ln[(\overline{c_1} - c_{eq})/(\overline{c_2} -$
 130 $c_{eq})]$ gave \bar{k} , where Γ is the volumetric flow rate per unit
 131 width, Δx is the streamwise distance between samples, $\overline{c_1}$ is
 132 the time-averaged concentration upstream, and $\overline{c_2}$ is the
 133 time-averaged concentration downstream.

[8] Images of surface slope, s , were obtained similar to
 135 previous studies [Jahne and Riemer, 1990], where a light
 136 source with an intensity gradient is placed beneath the
 137 waves and overhead images give measurements of slope.
 138 These images were collected at 125 frames per second. The
 139 term $\overline{s^2}$ denotes the mean square surface slope.

[9] Floating glass microballoons, of diameter 75 μm and
 141 effective density 0.18 g/cm^3 , acted as interfacial flow
 142 tracers. Just before images were collected they were dis-
 143 persed on the water surface. At low surface concentrations
 144 such as those used here, microballoons have been shown to
 145 change the surface conditions only negligibly [Kumar et al.,
 146 1998]. Images collected at 125 frames per second were fed
 147 into particle imaging velocimetry (PIV) calculations [Sveen,
 148 2004] to map the surface velocity field. Near-surface
 149 velocity obtained in this way was confirmed to agree with
 150 that from side-view images of neutrally buoyant particles.

[10] The airside friction velocity, u^* , was calculated by
 152 fitting time-averaged airside velocity profiles to a logarith-
 153 mic law assumption, i.e., $u^*/\kappa = d\overline{U}/d \log(z)$ where \overline{U} is the
 154 time-average wind speed, z is height above the mean surface
 155 level, and κ is the von Karman constant. U_{10} was calculated
 156 from u^* (and conversely) using correlations of Smith
 157 [1988], which, for our wind speeds, were recently reviewed
 158 and recommended [Yelland et al., 1998].

160 4. Results

[11] Examples of surface divergence fields are shown
 161 in Figures 1a–1d, where it is seen that well-organized
 162 patterns emerge above $u^* \sim 0.10 \text{ m/s}$. The pattern is periodic
 163 and in-phase with wave crests. Convergence zones appear
 164

165 just ahead of the crests and divergence zones just behind,
 166 confirming some results from side-view studies of micro-
 167 breaking waves [Peirson and Banner, 2003]. The patterns are
 168 not parallel-crested but are crescent shaped, similar to infra-
 169 red imagery captured in other studies [Zappa et al., 2001].

170 [12] The raw images of flow tracers, not shown here,
 171 afford additional qualitative information. For u^* greater than
 172 ~ 0.10 m/s, the tracers occasionally collect just downwind
 173 of a wave crest and “surf” along with the wave, i.e., travel
 174 at the crest velocity. This is evidence that water moves
 175 down the front of the wave at a speed equal to, or slightly
 176 greater than, the crest speed. This is a defining characteristic
 177 of wave breaking [Peirson and Banner, 2003]; Bubbles are
 178 not generated by this breaking. Such small wavelength
 179 breaking, which is ubiquitous on the ocean and on lakes,
 180 is often termed “microbreaking”. In our experiments it
 181 begins to occur at wavelengths of 5 cm ($u^* \sim 0.10$ m/s),
 182 simultaneous with the development of surface divergence
 183 patterns. We use the particle “surfing” behavior as an
 184 operational criterion for microbreaking.

185 [13] For each friction velocity a collection of 300 sequen-
 186 tial surface-velocity fields and 3750 sequential surface-slope
 187 fields were used for a calculation of $(\overline{\gamma^2})^{1/4}$ and s^2 respec-
 188 tively. The results are shown in Figure 2a where it is seen that
 189 the measures have similar shape, and show a change in
 190 behavior at $u^* \sim 0.10$ m/s when microbreaking begins. In
 191 Figure 2b, it is seen that $(\overline{\gamma^2})^{1/4}$ varies linearly with s^2 . It is

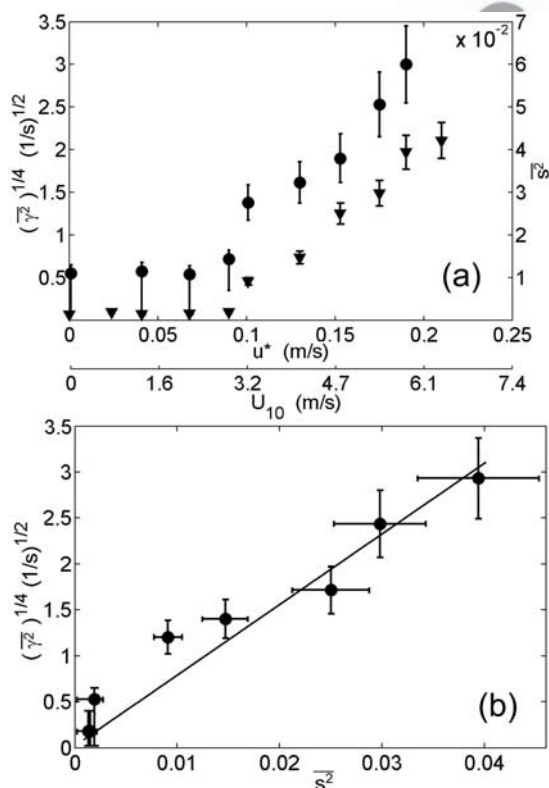


Figure 2. (a) The square root of rms surface divergence (circles) and the mean square slope (diamonds) are plotted versus friction velocity. A vertical offset, due to noise variance, is seen to affect the first few $(\overline{\gamma^2})^{1/4}$ values. (b) The linear relationship between $(\overline{\gamma^2})^{1/4}$ and s^2 is plotted with a linear regression, $r^2 = 0.93$.

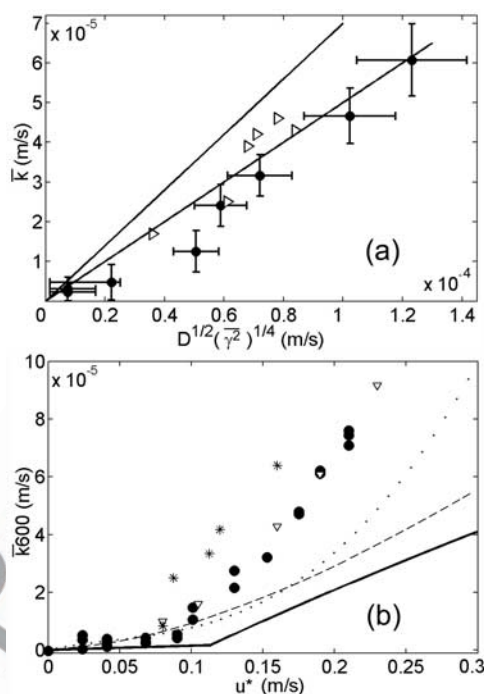


Figure 3. (a) The development of the gas transfer coefficient \bar{k} with $D^{1/2} (\overline{\gamma^2})^{1/4}$. A linear regression gives $\bar{k} = 0.45 D^{1/2} (\overline{\gamma^2})^{1/4}$, $r^2 = 0.95$. The solid lines are the prediction of equation (3), with $C = 0.7$ and 0.5 . Circles are data from this study. Right-pointing triangles are “cleaned II” data from the oscillating-grid tank study of McKenna and McGillis [2004]. (b) Gas transfer coefficients normalized to Sc of 600, $\bar{k}/600$, versus u^* (u^* is calculate from U_{10} as described in methods), compared with other experimental data and common oceanic parameterizations: Liss and Merlivat [1986] is the solid line; Nightingale et al. [2000] is the dashed line; Wanninkhof and McGillis [1999] is the dotted line; data of Komori et al. [1993] are the diamonds; data of Siddiqui et al. [2004] are the asterisks.

also seen that values of $(\overline{\gamma^2})^{1/4}$ level off at 0.5 (1/s)^{1/2} for 192
 lower wind speeds. This offset is due to small random PIV 193
 errors in γ , which are significant only at the lower wind 194
 speeds due to the $1/4$ exponent in $(\overline{\gamma^2})^{1/4}$. A correction for this 195
 effect is described in detail in the online supplemental 196
 material¹. All figures after Figure 2a use this corrected 197
 $(\overline{\gamma^2})^{1/4}$ data. Uncertainty in the final values of $(\overline{\gamma^2})^{1/4}$, s^2 , 198
 and \bar{k} are estimated by repeat experiments. 199

[14] In Figure 3a the surface divergence model is compared 200
 with our laboratory data. Values of \bar{k} are plotted against 201
 $D^{1/2} (\overline{\gamma^2})^{1/4}$ along with the grid-stirred tank data of McKenna 202
 and McGillis [2004]. Equation (3) is also plotted with $C =$ 203
 0.5 and $C = 0.7$, values suggested by direct numerical 204
 simulations in non-breaking conditions [Banerjee et al., 205
 2004] and by theory [McCready et al., 1986]. Figure 3a, 206
 shows that $D^{1/2} (\overline{\gamma^2})^{1/4}$ is a measure that can predict \bar{k} in a 207
 wide range of conditions, i.e., in grid-stirred tanks, at low 208
 wind speeds, and at intermediate wind speeds with breaking 209
 wavelets. There does exist an anomalous point in our data at 210

¹Auxiliary material is available at <ftp://ftp.agu.org/apend/gl/2004GL021671>.

211 $(\overline{\gamma^2})^{1/4} \sim 0.5$ and this will have to be the subject of future
212 investigation.

213 [15] Figure 3b shows \bar{k} values from laboratory experiments
214 as well as oceanic parameterizations. The data exhibit large
215 variability, which is to be expected since u^* is only indirectly
216 connected to \bar{k} . In spite of this variability, Figure 3b suggests a
217 change in gas transfer behavior at $u^* \sim 0.10$ m/s, near the
218 onset of breaking wavelets. Apparently, in both laboratory
219 and oceanic studies, the organized surface-normal motions of
220 microbreaking waves, seen in Figure 1, dominate the air-
221 water gas transfer process at intermediate wind speeds. Note
222 that, in Figure 3a, \bar{k} values from flow conditions of widely
223 different origin and character collapse to a single line.

224 [16] The gas transfer coefficients in Figure 3b are nor-
225 malized to a Schmidt number of 600 ($Sc = \nu/D$ where ν is
226 viscosity). This is done because this is the only way to
227 compare our results to data reported in the literature [Jahne
228 and Haussecker, 1998; Jahne et al., 1987; Wanninkhof and
229 McGillis, 1999]. However, if the surface divergence model
230 is accurate then normalization should only involve D , not
231 Sc . Experiments from McCreedy et al. [1986] confirm that
232 viscosity does not have a simple effect on \bar{k} .

233 [17] Turning now to measurements of mean square wave
234 slope, linear relationships between \bar{k} and s^2 have been found
235 in previous studies [Jahne et al., 1987], and were confirmed
236 here; data are in the online material. In light of our experi-
237 ments, this result can be expected based on the combination
238 of Figures 2b and 3b, showing that s^2 is linearly correlated
239 with $(\overline{\gamma^2})^{1/4}$ and $(\overline{\gamma^2})^{1/4}$ is linearly correlated with \bar{k} . The
240 hydrodynamic reason for the linear correlation between s^2
241 and $(\overline{\gamma^2})^{1/4}$ is unclear at present, but the relationship in
242 Figure 2b provides some insight. A connection between s^2
243 and \bar{k} is intriguing since surface roughness measurements,
244 such as slope, may be gathered over large spatial areas using
245 satellite remote sensing. We caution that in field conditions,
246 with fetch, swell, and other complexities, the relationship
247 between s^2 and $(\overline{\gamma^2})^{1/4}$ could easily be different than
248 Figure 2b. However, even if our laboratory wave conditions
249 are much different than the real ocean, there is no reason to
250 expect the surface divergence model, equation (3), to fail in
251 field settings, as long as the interface is clean and bubbles
252 are not present.

253 5. Summary

254 [18] Our results support the surface divergence model of
255 air-water gas transfer in low and intermediate wind speeds,
256 with microbreaking wavelets. Taken with the results of
257 McKenna and McGillis [2004] and Banerjee et al. [2004],
258 the surface divergence model agrees with experiments over a
259 wide range of conditions. Linear relationships are found
260 between \bar{k} and $(\overline{\gamma^2})^{1/4}$, and also between s^2 and $(\overline{\gamma^2})^{1/4}$,
261 explaining previously observed correlations between s^2 and
262 \bar{k} . Microbreaking waves commence forming at $u^* \sim 0.10$ m/s,
263 equivalent to $U_{10} \sim 3.5$ m/s, and significantly increase the
264 surface-normal motions in the concentration boundary layer,
265 as seen in Figure 1. These motions dominate the gas transfer
266 process at intermediate wind speeds, likely causing the
267 regime change seen in Figure 3b.

268 [19] **Acknowledgments.** We would like to acknowledge early work
269 done on this problem by Dr. Ira Leifer, Brian Pirorek, and Emma Perez. This
270 work was supported by DOE grant DE-FG03-85ER13314.

References

- Banerjee, S. (1990), Turbulence structure and transport mechanisms at
272 interfaces, in *Ninth International Heat Transfer Conference*, pp. 395–
273 418, Hemisphere Press, New York. 274
- Banerjee, S., and S. MacIntyre (2004), The air-water interface: Turbulence
275 and scalar exchange, in *Advances in Coastal and Ocean Engineering*,
276 edited by P. L. F. Liu, pp. 181–237, World Sci., Hackensack, N. J. 277
- Banerjee, S., D. Lakehal, and M. Fulgosi (2004), Surface divergence models
278 for scalar exchange between turbulent streams, *Int. J. Multiphase Flow*,
279 30(7-8), 963–977. 280
- Chan, W. C., and L. E. Scriven (1970), Absorption into irrotational stagna-
281 tion flow: A case study in convective diffusion theory, *Ind. Eng. Chem.*
282 *Fundam.*, 9(1), 114–120. 283
- Csanady, G. T. (1990), The role of breaking wavelets in air-sea gas transfer,
284 *J. Geophys. Res.*, 95(C1), 749–760. 285
- Danckwerts, P. V. (1951), Significance of liquid-film coefficients in gas
286 absorption, *Ind. Eng. Chem.*, 43(6), 1460–1467. 287
- Donelan, M. A., W. M. Drennan, E. S. Saltzman, and R. Wanninkhof (Eds.)
288 (2002), *Gas Transfer at Water Surfaces*, *Geophysical Monogr. Ser.*, vol.
289 127, pp. 1–10, AGU, Washington, D.C. 290
- Jahne, B., and H. Haussecker (1998), Air-water gas exchange, *Annu. Rev.*
291 *Fluid Mech.*, 30, 443–468. 292
- Jahne, B., and K. S. Riemer (1990), Two-dimensional wave number spectra
293 of small-scale water-surface waves, *J. Geophys. Res.*, 95(C7), 11,531–
294 11,546. 295
- Jahne, B., K. O. Munnich, R. Bosinger, A. Dutzi, W. Huber, and P. Libner
296 (1987), On the parameters influencing air-water gas exchange, *J. Geo-*
297 *phys. Res.*, 92(C2), 1937–1949. 298
- Komori, S., R. Nagaosa, and Y. Murukami (1993), Turbulence structure and
299 mass transfer across a sheared air-water interface in wind-driven turbu-
300 lence, *J. Fluid Mech.*, 249, 161–183. 301
- Kumar, S., R. Gupta, and S. Banerjee (1998), An experimental investiga-
302 tion of the characteristics of free-surface turbulence in channel flow,
303 *Phys. Fluids*, 10(2), 437–456. 304
- Liss, P. S., and L. Merlivat (1986), Air-sea gas exchange rates: Introduction
305 and synthesis, in *The Role of Air-Sea Exchange in Geochemical Cycles*,
306 edited by P. Buat-Menard, pp. 113–127, Springer, New York. 307
- McCreedy, M. J., and T. J. Hanratty (1985), Effect of air shear on gas-
308 absorption by a liquid-film, *AIChE J.*, 31(12), 2066–2074. 309
- McCreedy, M. J., E. Vassiliadou, and T. J. Hanratty (1986), Computer-
310 simulation of turbulent mass-transfer at a mobile interface, *AIChE J.*,
311 32(7), 1108–1115. 312
- McKenna, S. P., and W. R. McGillis (2004), The role of free-surface turbu-
313 lence and surfactants in air-water gas transfer, *Int. J. Heat Mass Transfer*,
314 47(3), 539–553. 315
- Nightingale, P. D., G. Malin, C. S. Law, A. J. Watson, P. S. Liss, M. I.
316 Liddicoat, J. Boutin, and R. C. Upstill-Goddard (2000), In situ evaluation
317 of air-sea gas exchange parameterizations using novel conservative and
318 volatile tracers, *Global Biogeochem. Cycles*, 14(1), 373–387. 319
- Peiron, W. L., and M. L. Banner (2003), Aqueous surface layer flows
320 induced by microscale breaking wind waves, *J. Fluid Mech.*, 479, 1–38. 321
- Siddiqui, M. H. K., M. R. Loewen, W. E. Asher, and A. T. Jessup (2004),
322 Coherent structures beneath wind waves and their influence on air-water
323 gas transfer, *J. Geophys. Res.*, 109, C03024, doi:10.1029/2002JC001559. 324
- Smith, S. D. (1988), Coefficients for sea-surface wind stress, heat flux, and
325 wind profiles as a function of wind speed and temperature, *J. Geophys.*
326 *Res.*, 93, 15,467–15,472. 327
- Sveen, J. K. (2004), An introduction to MatPIV v.1.6.1, in *Mechanics and*
328 *Applied Mathematics*, pp. 27, Dept. of Math., Univ. of Oslo, Oslo. 329
- Takahashi, T., et al. (2002), Global sea-air CO₂ flux based on climatological
330 surface ocean pCO₂, and seasonal biological and temperature effects,
331 *Deep-Sea Res., Part II*, 49(9-10), 1601–1622. 332
- Wanninkhof, R. H., and W. R. McGillis (1999), A cubic relationship between
333 air-sea CO₂ exchange and wind speed, *Geophys. Res. Lett.*, 26(13), 1889–
334 1892. 335
- Yelland, M. J., B. I. Moat, P. K. Taylor, R. W. Pascal, J. Hutchings, and
336 V. C. Cornell (1998), Wind stress measurements from the open ocean
337 corrected for airflow distortion by the ship, *J. Phys. Oceanogr.*, 28(7),
338 1511–1526. 339
- Zappa, C., W. E. Asher, and A. Jessup (2001), Microscale wave breaking
340 and air-water gas transfer, *J. Geophys. Res.*, 106(C5), 9385–9391. 341
- S. Banerjee, Department of Chemical Engineering, University of
342 California, Santa Barbara, CA 93106, USA. 344
- W. C. Smith, Department of Mechanical and Environmental Engineering,
345 University of California, Santa Barbara, CA 93106, USA. 346
- D. E. Turney, Bren School of Environmental Science and Management,
347 University of California, Santa Barbara, CA 93106, USA. (dturney@
348 bren.ucsb.edu) 349